Available online at www.sciencedirect.com
ScienceDirect
Deep-Sea Research I 55 (2008) 608–629
DEEP-SEA RESEARCH PART I
www.elsevier.com/locate/dsri

# Geostrophic circulation between the Costa Rica Dome and Central America

C.L. Brenes[a], M.F. Lavín[b,*,1], Affonso S. Mascarenhas Jr.[c]

[a]*Servicio Regional de Información Oceanográfica, Universidad Nacional, Heredia, Costa Rica*
[b]*Departamento de Oceanografía Física, CICESE, Km. 107 Carretera Tijuana-Ensenada, Ensenada, Baja California, Mexico*
[c]*Instituto de Investigaciones Oceanológicas, Universidad Autónoma de Baja California, Baja California, Mexico*

Received 26 January 2007; received in revised form 23 January 2008; accepted 7 February 2008
Available online 4 March 2008

**Abstract**

The geostrophic circulation between the Costa Rica Dome and Central America is described from CTD observations collected in two surveys: (a) The Wet Cruise in September–October 1993, and the Jet Cruise in February–March 1994. Poleward coastal flow was present on both occasions, but the transition from flow around the dome to the poleward Costa Rica Coastal Current flow was quite tortuous because of the presence of mesoscale eddies. In particular, a warm anticyclonic eddy was found off the Gulf of Fonseca during both cruises, at an almost identical position and with similar dimensions (150 m deep, 250 km in diameter) and surface speed (0.5 m $s^{-1}$). In the Gulf of Panama, poleward flow was also observed, weaker in February–March 1994 than in September–October 1993, when it penetrated to 600 m depth and transported 8.5 Sv. In September–October 1993, the current between the dome and the coast was mostly ~100 m deep and weak (~0.15 m $s^{-1}$), although in its southern side it was deeper (~450 m) and faster at 0.3 m $s^{-1}$. The poleward transport between the dome and the coast was ~7 Sv. In February–March 1994 the Costa Rica Dome was a closed ring adjacent to the continental shelf, ~500 km in diameter, at least 400 m deep, had geostrophic surface speeds ~0.25 m $s^{-1}$, and subsurface maximum speed (0.15–0.20 m $s^{-1}$) at ~180 m depth; the associated uplift of the isotherms was ~150 m. The flow in the south part of the dome splits into two branches, the weakest one going around the dome and the strongest one continuing east and turning south before reaching the Gulf of Panama.


*Keywords:* Geostrophic circulation; Costa Rica Dome; Costa Rica coastal Current

## 1. Introduction

The basic oceanography of the eastern tropical Pacific, off the coast of Central America (Fig. 1) is summarized in the classic compilations of Wyrtki (1965, 1966, 1967) and recently updated by Kessler (2006) and Fiedler and Talley (2006). These works provide a description of the distribution and seasonal variability of the water masses and of the system of currents in the eastern tropical Pacific.

*Corresponding author. Tel.: +52 646 175 0500x24061; fax: +52 646 175 0547.
*E-mail addresses:* cbrenes@una.ac.cr (C.L. Brenes), mlavin@cicese.mx (M.F. Lavín), asmj@uabc.mx (A.S. Mascarenhas Jr.).
[1]Postal address: CICESE-Oceanography, P.O. Box 434844, San Diego, CA 92143-4844, USA.

0967-0637/$ - see front matter © 2008 Elsevier Ltd. All rights reserved.
doi:10.1016/j.dsr.2008.02.005

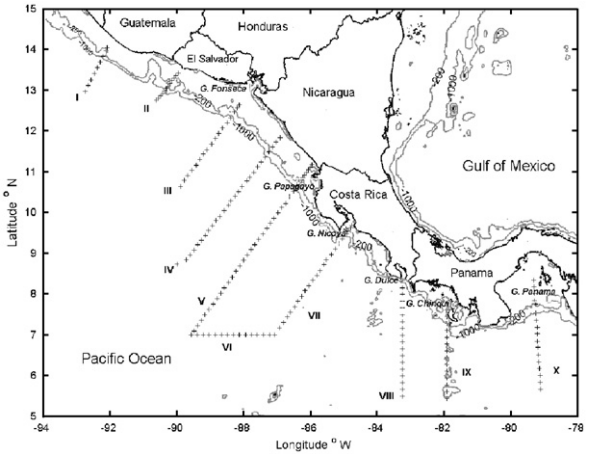


Fig. 1. Eastern Tropical Pacific off Central America, with the oceanographic sections, in Roman numerals I to X, and geographical locations.

In the last 20 years, research on the oceanography of the eastern tropical Pacific has tended to focus on the upwelling and eddies generated by the wind jets that blow across mountain gaps in southern Mexico and Central America, and to a lesser extent on the Costa Rica Dome (CRD) and the Costa Rica Coastal Current (CRCC), which are more permanent features. Upwelling in the eastern tropical Pacific, specifically in the CRD and in the gulfs of Tehuantepec, Papagayo and Panama, supports important fisheries (Fiedler, 2002).

The near-surface hydrography and circulation in the eastern tropical Pacific are strongly affected by local air–sea interaction. There is a seasonal signal in most oceanographic features of the region, related to the north–south migration of the Inter-Tropical Convergence Zone (ITCZ). Not only are the surface temperature and salinity controlled by local heat fluxes and precipitation-minus-evaporation rates, but the circulation is driven by the seasonally variable wind field (Kessler, 2006). The zone of maximum precipitation in the eastern tropical Pacific follows the position of the ITCZ (Amador et al., 2006); consequently the seasonal minimum precipitation in Central America occurs in April–May and the maximum in October–November. The seasonal evolution of the wind field also follows the ITCZ, with the added richness of three mountain-pass jets that blow between November and March: the Tehuantepec Jet, the Papagayo Jet and the Panama Jet (Chelton et al., 2000; Chelton and Esbensen, 2000). Although the wind jets occur only in the boreal winter, they imprint the climatological wind and sea surface temperature (SST) distributions, as well as the circulation (Kessler, 2006; Fiedler and Talley, 2006). On the right flank of each jet (looking downwind) the wind stress curl is negative, leading to downwelling, which can in turn produce warm anticyclonic eddies; this is well established by models and by direct observation for the Tehuantepec eddies (Clarke, 1988; McCreary et al., 1989; Umatani and Yamagata, 1991; Barton et al., 1993; Trasviña et al., 1995). On the left flank of the jets, the vertical Ekman pumping caused by the positive wind stress curl lifts the thermocline; this can lead to the generation of cool cyclonic eddies (see review by Willett et al., 2006) and in the case of the Papagayo Jet, to the generation of the CRD (Fiedler, 2002; Kessler, 2006).

The CRD is an offshore upwelling center characterized by an uplift of the thermocline, centered around 9°N, 90°W. Recent studies by Fiedler (2002) and Kessler (2002, 2006) have shed considerable light on the mean and seasonal evolution of, and the basic mechanisms responsible for, the CRD. Fiedler (2002) describes the seasonal evolution of the CRD and shows its close association with that of the wind stress curl. Kessler (2002) has proved that in the mean the CRD is due to the dipolar wind stress curl distribution created by the Papagayo Jet and the south trade winds, which are southwesterly in that zone.

According to Wyrtki (1965), the CRCC starts between the CRD and the coast, and its seasonal behavior is as follows: from January to March it flows to the west between 9 and 12°N, in April and May it leaves the coast at the Gulf of Tehuantepec, in June–July it flows along the coast as far as Cape Corrientes, and from August to December it leaves the coast after passing the Gulf of Tehuantepec. The start of the CRCC at the Dome is present in the analyses of Fiedler (2002) and Kessler (2002, 2006). Nevertheless, neither the geostrophic nor the drifter velocities (Kessler, 2006; Figs. 2 and 4) show the surface CRCC continuing north past the Gulf of Tehuantepec.

The works of Fiedler (2002) and Kessler (2002, 2006) are based on the analysis of historical data banks (SST, temperature profiles, ship drift) and recent drifter and satellite data, notably wind speed from scatterometers (ERS 1/2 and QuikScat), which allow the calculation of the curl of the wind stress with the horizontal resolution necessary to resolve the jets (Chelton et al., 2004). Surprisingly,

considering the oceanographic importance of the region, there are no works describing the structure of the CRCC, and the only reported surveys on the CRD are those of Wyrtki (1964) and the four Mexican 1979–1982 DOMO cruises (Barberán et al., 1985).

This article aims to further the regional oceanographic knowledge of the region off the Pacific coast of Central America. Hydrographic data from two detailed surveys are used to describe the geostrophic current field in the region between the coast and the CRD, both to give support to the recent findings based on averaged data and to add the details that such an approach misses, like the structure of the CRCC, the circulation formed by the NECC as it reaches the eastern boundary, and the structure and effects of mesoscale eddies.

## 2. Data and methodology

The temperature ($T$) and salinity ($S$) profiles used here were collected in two surveys (Fig. 1) made on the R/V *Fengur*, the first from September 25 to October 18, 1993, and the second from February 25 to March 10, 1994. Since the first cruise was made in the middle of the rainy season, and the second at the time when the jets are present, we will refer to the cruises as the Wet Cruise and the Jet Cruise, respectively. The cruises also fall in the two extremes of the seasonal evolution of the CRD (described in Section 3). The stations were made on nine transects normal to the coast, from Guatemala to Panama, and one zonal transect (at 7°N); these sections and the geographic features and locations mentioned in the text are shown in Fig. 1. The distance between stations ranged from 15 km over the continental shelf and slope to 25–35 km offshore, thus well below the internal Rossby radius of deformation for the region (80–150 km, according to Chelton et al., 1998). A MER CTD was lowered down to ~900 m in the Wet Cruise and to ~500 m in the Jet Cruise (the CTD cable had to be cut).

The salinity data from the two cruises were corrected so that the $T$–$S$ diagrams of each section were centered on the Levitus climatology for the area at temperatures below 13 °C (that is, below the thermocline, which is found at 100–200 m depth). This was necessary because the original CTD calibration data were not available. The corrected $T/S$ diagrams from the two cruises (Fig. 2) show that the CTD salinity from the second (Jet) cruise had a wider variability than in the first (Wet) cruise,

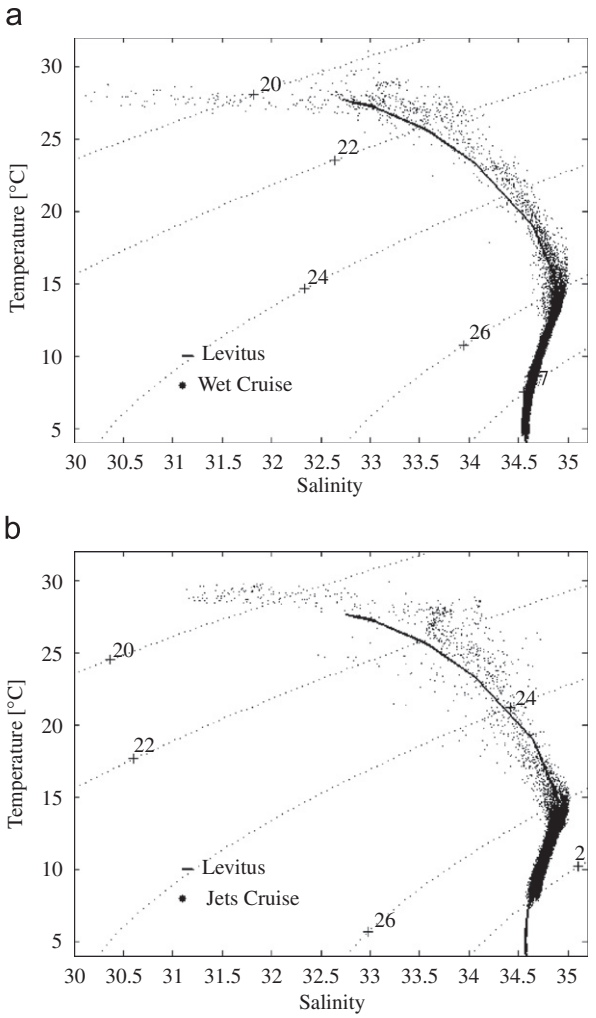


Fig. 2. $T$–$S$ diagrams for (a) Wet Cruise, (b) Jet Cruise. Continuous line is the mean $T$–$S$ diagram from the Levitus climatology for the zone.

presumably from instrument noise. Although the salinity corrections and the variability do not have an important effect on the geostrophic velocity calculations, slight salinity variations indicative of water masses are not accurate enough for the Jet Cruise.

Vertical sections of geostrophic velocity were calculated from the $T$ and $S$ profiles and then smoothed by objective analysis using a Gaussian covariance function in order to remove the effect of internal waves and other small-scale variability; the vertical scale was 30 m, while the horizontal scale varied with the length of the section. The horizontal scales are listed in Table 1 (column 1). The level of no motion was the deepest common sampled depth in pairs of stations. The effect of the different

Table 1
Volume transport in Sverdrups ($1\,Sv = 10^6\,m^3\,s^{-1}$) by geostrophic currents relative to minimum common depth: ~900 m (500 m) for offshore stations in Wet (Jet) Cruise. For the Wet Cruise, the second row gives transport above 500 m using 500 m as level of no motion

| Section $L_x$ (km) | Jet Cruise: February 25–March 10, 1994 | | Wet Cruise: September 25–October 18, 1993 | |
|---|---|---|---|---|
| | Poleward Transport | Equatorward Transport | Poleward Transport | Equatorward Transport |
| I | 0.6 | −0.9 | 3.6 | −0.3 |
| 50 | | | 1.0 | −0.4 |
| II | 1.7 | −0.1 | 2.2 | −0.6 |
| 30 | | | 1.5 | −0.5 |
| III | 4.6 | −5.5 | 9.3 | −5.7 |
| 70 | | | 6.4 | −5.0 |
| IV | 3.5 | −1.9 | 7.0 | −3.0 |
| 110 | | | 5.2 | −1.0 |
| V | 7.4 | −15.6 | 6.7 | −7.6 |
| 150 | | | 3.3 | −5.1 |
| VII | 3.7 | −4.3 | 5.2 | −2.3 |
| 110 | | | 3.4 | −2.4 |
| VIII | 2.9 | −5.5 | 10.9 | −7.9 |
| 110 | | | 4.0 | −5.6 |
| IX | 1.7 | −2.5 | 3.6 | −3.7 |
| 110 | | | 3.1 | −2.8 |
| X | 2.4 | −1.9 | 8.5 | −1.9 |
| 150 | | | 4.6 | −0.9 |

Objectively analyzed geostrophic velocities shown in Figs. 5 and 8 were used. Calculations were made only for speeds faster than $\pm 0.05\,ms^{-1}$. Horizontal ($L_x$) scales of decay used in the objective analysis were chosen depending on the length of the section, and are given in column one; the vertical ($L_z$) scale was 30 m in all cases.

sampling depths for the two cruises is discussed later.

## 3. Results and discussion

In order to frame our observations in the seasonal evolution of the wind, hydrography and geostrophic current fields off Central America, we first summarize the description given by Fiedler (2002) of the evolution of the wind field and the CRD. It can be separated into five stages. *February–April* (Stage 1): The ITCZ is in its southernmost position, northeasterly trades and the Papagayo Jet are blowing strong, and the wind stress curl lifts the thermocline close to the coast on the equatorward side of the Papagayo Jet; this is the generation stage of the CRD. The North Equatorial Counter Current (NECC), and consequently the CRCC, are absent. *May–June* (Stage 2): The ITCZ has shifted north, so that the southerly trades start affecting the area, the Papagayo Jet stops, and the still weak CRD separates from (but remains close to) the coast. The NECC starts flowing on the southern flank of the CRD, extends to the coast and turns to feed the CRCC. *July–October* (Stage 3): Southerly trades remain strong in the area, with a band of cyclonic wind stress curl on the poleward side of the ITCZ, above the NECC thermocline ridge; this causes the ridge to shoal. The CRD expands west over the shoaling ridge (from a length of 300 km in June to 1000 km in November) and along the band of positive wind stress curl of the ITCZ. *November* (Stage 4): The ITCZ moves south, and the Tehuantepec Jet starts. The positive curl on the equatorial side of the Tehuantepec Jet causes the northern side of the CRD to shoal. *December–January* (Stage 5): The ITCZ and its band of positive wind stress curl move south of the NECC ridge, while strong northeasterly trades blow over the CRD. The CRD weakens and shrinks, decaying while the genesis of the new dome is already taking place close to the coast.

To follow the seasonal evolution, the results of the Jet Cruise (Stage 1, as described above) are presented first, and then those of the Wet Cruise (Stage 3).

### 3.1. The Jet Cruise (February 25 to March 10, 1994)

#### 3.1.1. Surface distributions

The overall SST distribution during the Jet Cruise given by the 8-day mean AVHRR-derived SST (Fig. 3a) shows that the Papagayo and Panama Jets were blowing (a fact sorely attested to by the cruise participants). The surface cold tongues generated under these jets are clearly visible, separated by a high-SST zone. If the CRD were present, its SST signature probably would have been masked by the SST minimum caused by the Papagayo Jet. The black line in Fig. 3a is the edge of the CRD, according to Fiedler (2002), defined as the locus of the 35 m depth of the 20 °C isotherm. This isotherm is usually in the center of the thermocline in the eastern tropical Pacific (Kessler, 2002; Fiedler and Talley, 2006).

The CTD-derived distributions of temperature, salinity, depth of the thermocline and surface dynamic height (relative to 500 m) are shown in Fig. 4, with the Stage 1 CRD position (shaded), according to Fiedler (2002). The SST (Fig. 4a)

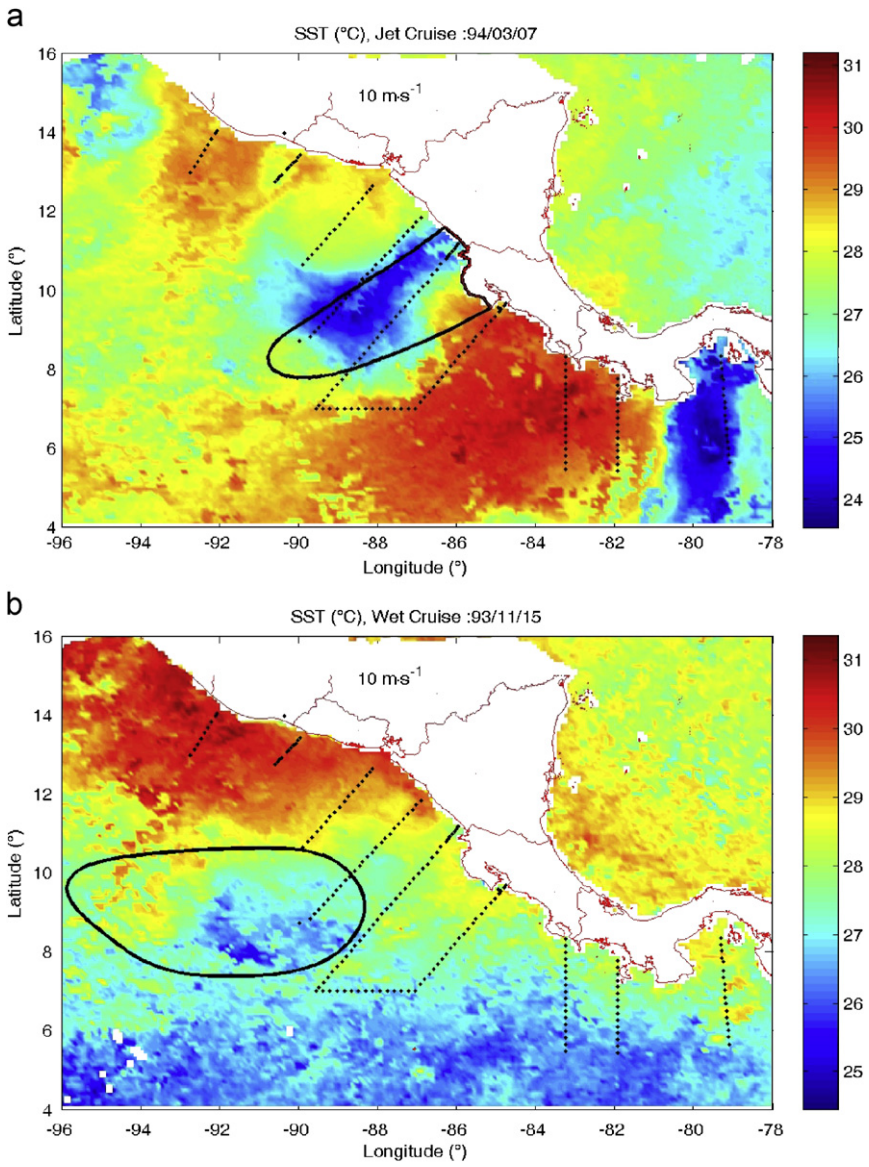


Fig. 3. Mean AVHRR SST distributions during the weeks centered on: (a) March 7, 1994, during the Jet Cruise, (b) September 15, 1993, during the Wet Cruise. The satellite AVHRR data are eight-day means, 9 km spatial resolution, version 4.0, obtained from http://podaac.jpl.nasa.gov. The black line is the climatological position of the Costa Rica Dome for February and September, according to Fiedler (2002).

shows circular isotherms surrounding an offshore minimum; they are closed on the land side and open offshore. There are two zones of minimum SST ($<24\,^{\circ}C$), in the Gulf of Panama and off Costa Rica, the latter centered at 9°N, 89°W, in the offshore extreme of section IV. The two minimum SST areas are separated by an area with high SST ($\sim29\,^{\circ}C$), and there is also high SST ($>28\,^{\circ}C$) in the northern extreme of the sampled area. These areas of high SST are part of the Western Hemisphere Warm Pool of the Eastern Pacific (Wang and Enfield, 2001, 2003), which in this season (and on average) is cut by the low SST generated by the jets (Fiedler and Talley, 2006). On the edges of the minimum SST (Fig. 4a) the isotherms are normal to the coast and form a strong zonal gradient, which is also seen in Fig. 3a.

The sea surface salinity (Fig. 4b) shows a high (~34.5) in the middle of section V and in the extreme of section IV, while further to the NW it is

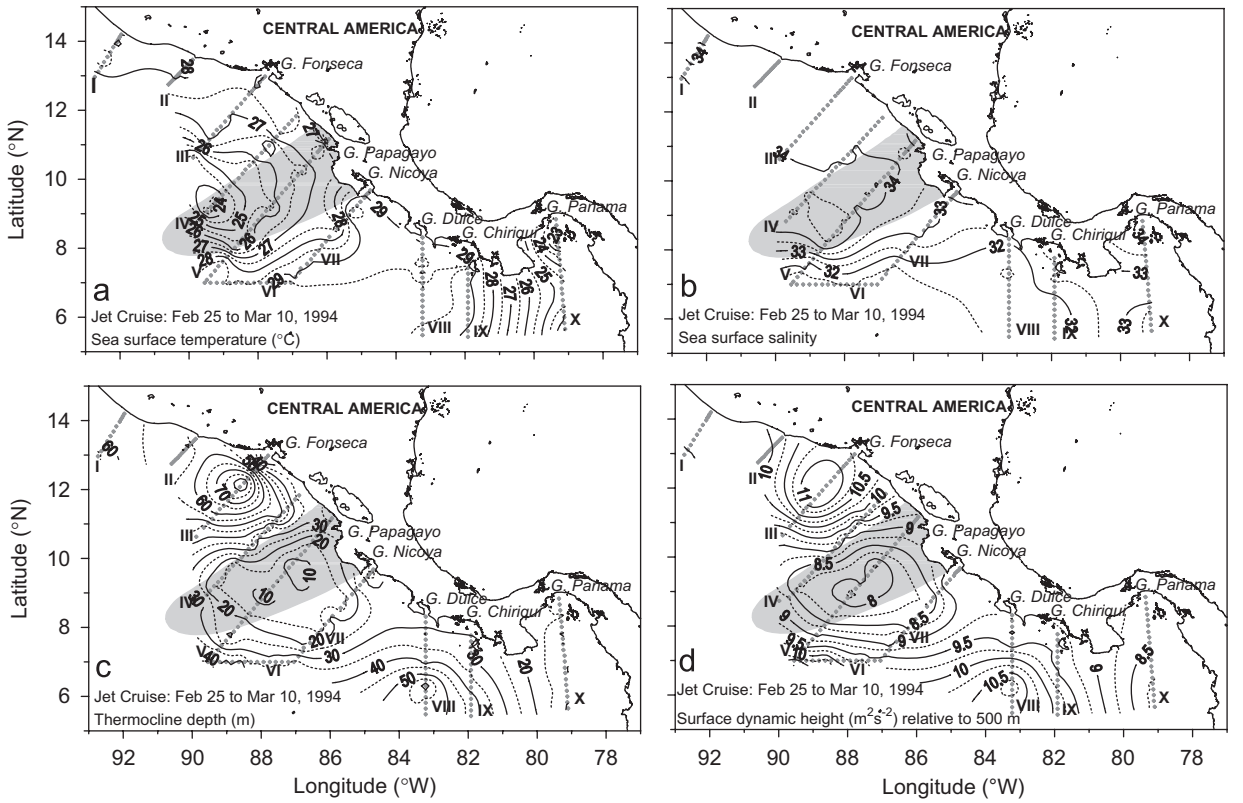


Fig. 4. Horizontal distributions from CTD data, during the Jet Cruise, February–March 1994: (a) SST in °C, (b) Sea surface salinity, (c) Thermocline depth in m (depth of 20 °C isotherm), (d) dynamic height of the surface relative to 500 m, in $m^2 s^{-2}$. Shading is the climatological position of the Costa Rica Dome for February, according to Fiedler (2002).

33.6–33.8, which is a mean value for the zone and time of the year (Fiedler and Talley, 2006).

The distribution of the thermocline depth (depth of the 20 °C isotherm, Fig. 4c) is configured as a sequence of dipoles. The northern low-high pair (or dipole) is attached to the coast, with its depression (max. 80 m) off the Gulf of Fonseca, but with a larger area of uplift (~10 m) off the Gulf of Papagayo. The southern couple has its maximum depression (55 m) off the Gulf of Chiriquí and its uplift (min. ~10 m) in the Gulf of Panama. The surface dynamic height (relative to 500 m, Fig. 4d) reflects the two dipoles present in the thermocline topography. Thus the main circulation features in the dynamic topography are: (a) cyclonic circulation around the CRD off the Gulf of Papagayo, (b) an anticyclonic eddy off the Gulf of Fonseca, (c) anticyclonic flow off Golfo Dulce, (d) cyclonic flow in the Gulf of Panama, and (e) offshore flow off Gulf of Chiriquí, made evident by the eastward decrease of the dynamic height between sections VIII and X. The poleward flow between the CRD and the coast, from which the CRCC is supposed to originate, meets the equatorward flow of the Fonseca eddy, forcing it to flow offshore; its fate afterwards cannot be determined here, but evident possibilities are its reattachment to the coast after circling the eddy or its joining the westward North Equatorial Current. The CRCC is not apparent in Fig. 4d because the coastal stations are excluded by the 500 m reference level, but we will see in the geostrophic velocity (below) that there is a coastal poleward flow through most sections.

### 3.1.2. *Vertical sections of geostrophic velocity*

Fig. 5 shows the vertical distribution of geostrophic velocity ($V_g$) during the Jet Cruise, assuming no motion at the deepest common depth of adjacent stations (~500 m in the offshore stations), with positive values (in Fig. 5, dark gray for values $>0.05\,m\,s^{-1}$) meaning flow into the page: poleward for sections I–V and VII, northward in section VI, and westward in sections VIII to X. The corresponding positive (poleward/westward) and negative

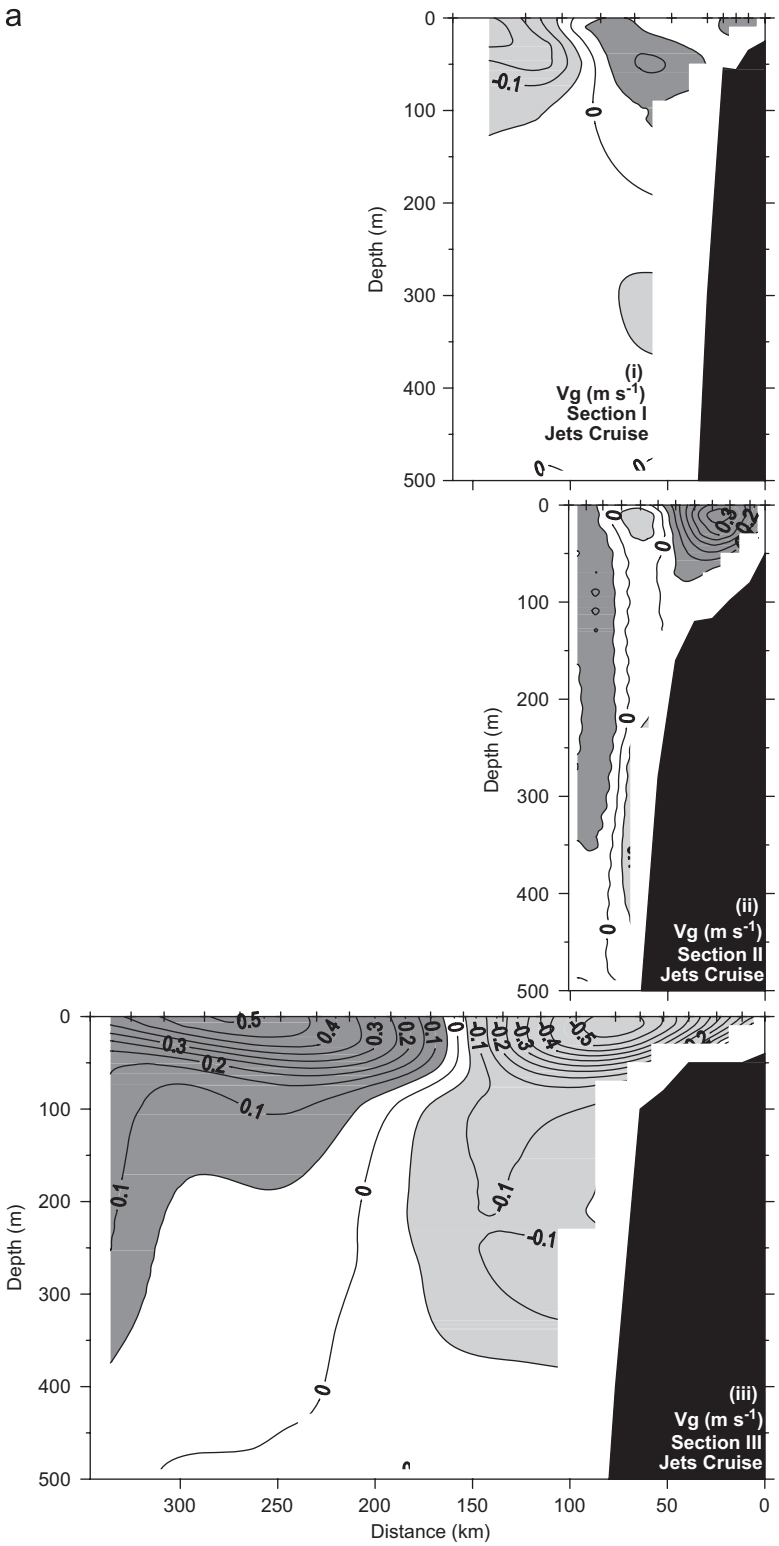


Fig. 5. Vertical distribution of geostrophic velocity ($V_g$, m s$^{-1}$) relative to 500 m (or to deepest common depth), for the Jet Cruise: (i) section I, (ii) section II, (iii) section III, (iv) section IV, (v) section V, (vi) section VI, (vii) section VII, (viii) section VIII, (ix) section IX, (x) section X. Positive velocity (into the page) above 0.05 m s$^{-1}$ is shaded. Ticks in the top axis are the CTD stations.

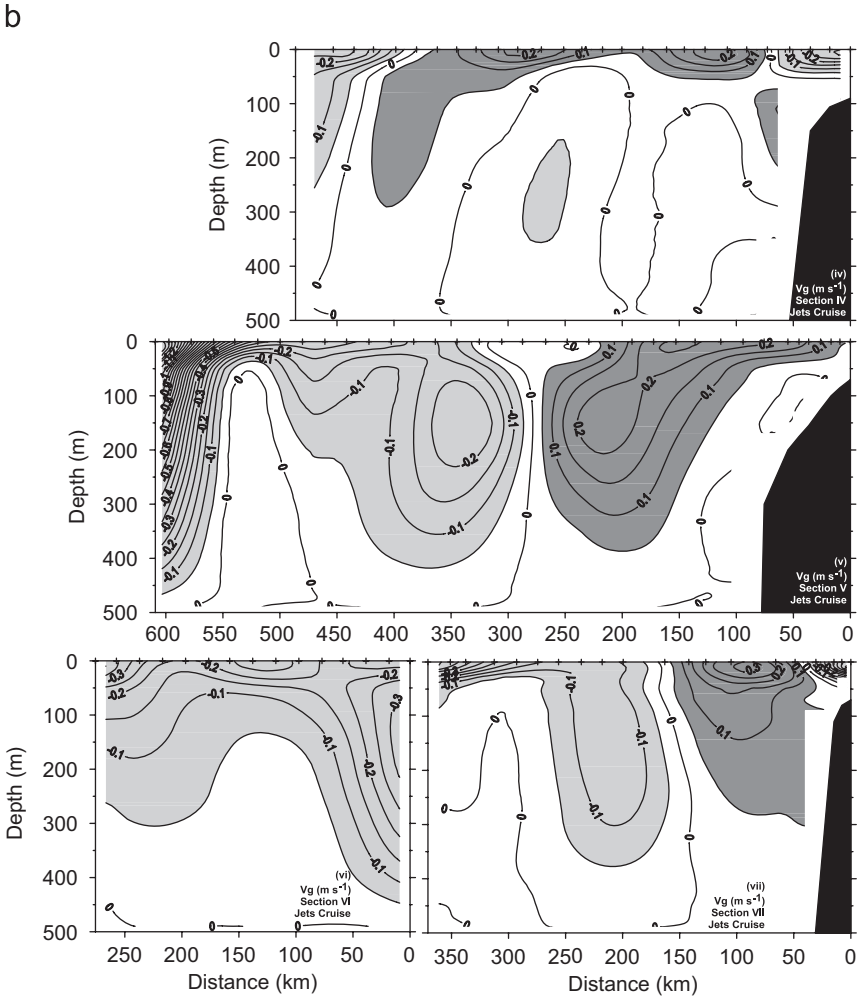


Fig. 5. (*Continued*)

(equatorward/eastward) transports, for speeds faster than $\pm 0.05\,m\,s^{-1}$, are shown in Table 1.

The geostrophic velocity across Section I (Fig. 5i) shows poleward flow ($\sim 0.1\,m\,s^{-1}$) in the top 100 m for some 50 km beyond the shelf break, and then equatorward flow in the top 100 m, with maximum speed $\sim 0.2\,m\,s^{-1}$ in the surface. In section II (Fig. 5ii) there is poleward flow with speed $\sim 0.3\,m\,s^{-1}$ over the shelf (reaching $\sim 100$ m depth), followed by weak ($\sim 0.05\,m\,s^{-1}$) equatorward flow in the top 50 m and also between 300 and 450 m depth. Further seaward, there is poleward flow again, although weak ($\sim 0.1\,m\,s^{-1}$) and deep ($\sim 350$ m). The poleward flow in sections I and II could be interpreted as the CRCC, but it is narrower than in the Wyrtki (1965) diagrams, and the transport is low, 0.6 and 1.7 Sv, respectively (Table 1).

The geostrophic flow in section III (Fig. 5iii) shows that the anticyclonic eddy off the Gulf of Fonseca had speeds reaching $0.5\,m\,s^{-1}$ in the surface and $\sim 0.1\,m\,s^{-1}$ at 100 m, but speeds around $0.05\,m\,s^{-1}$ are observed down to 400 m; the transports are $\sim 5$ Sv in both directions (Table 1). The currents in section IV (Fig. 5iv), being located in the transition from the Fonseca eddy to the CRD, reflect circulation from both features in agreement with the dynamic height distribution (Fig. 4d).

The geostrophic velocity across Section V (Fig. 5v) shows a tight cyclonic circulation around the CRD. There is poleward flow from the coast to $\sim 300$ km offshore, with maximum speeds $\sim 0.2\,m\,s^{-1}$ in the surface. The southward branch of the flow around the CRD extends from 300 to 650 km offshore, with maximum surface speed

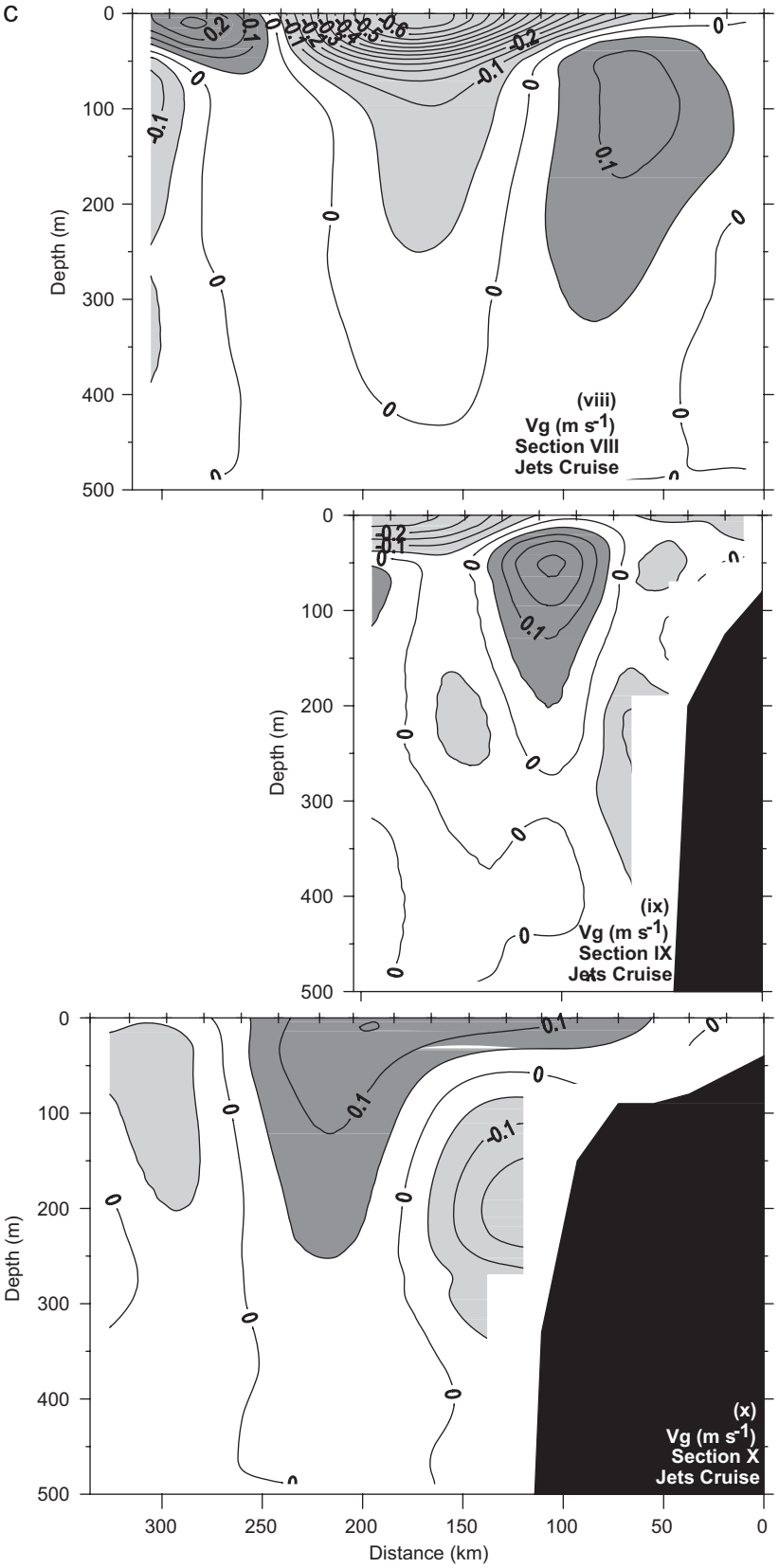


Fig. 5. (*Continued*)

$\sim$0.2 m s$^{-1}$. On both sides of the dome there are subsurface cores of relative maximum speeds ($\sim$0.2 m s$^{-1}$) at 200 m depth. The depth of the gyre is $\sim$400 m, but as shown below, it probably was deeper. The transport involved in the cyclonic circulation is $\sim$7 Sv (Table 1).

The zonal section VI and section VII both cut the edge of the CRD, as shown in the dynamic height distribution (Fig. 4d). The geostrophic currents in the former (Fig. 5vi) show fast equatorward flow in the top 400 m, reaching 0.25 m s$^{-1}$ in the surface; since this is the northward component of a mostly eastward flow (see Fig. 4d), the current must have been faster than 0.25 m s$^{-1}$. Section VII (Fig. 5vii) shows the cyclonic flow of the CRD, in accordance to section V, but with transport $\sim$4 Sv (Table 1).

The meridional sections VIII and IX (Fig. 5viii and ix) show a shallow ($<$100 m) and fast (0.3–0.5 m s$^{-1}$) surface eastward (negative) flow transporting $\sim$5 Sv (Table 1) and a westward (positive) subsurface flow with a core of maximum speed around 0.1–0.2 m s$^{-1}$, transporting 2.9 Sv (Table 1). Section IX also has weak ($\sim$0.05 m s$^{-1}$) eastward flow over the shelf and slope, including a subsurface jet attached to the continental slope at depths between 200 and 400 m. The shallow surface eastward flow was apparent in the dynamic height distribution (Fig. 4d), which suggests that it is connected to the eastward flow in the south edge of the CRD. Note that for section IX, Fig. 5ix shows, at the surface, the eastward component of a mostly southward flow, as indicated by the dynamic topography (Fig. 4d).

The geostrophic velocity off the Gulf of Panama, Section X (Fig. 5x), shows westward flow ($\sim$0.1 m s$^{-1}$; 2.4 Sv) from the surface to about 200 m, and a 50 km-wide subsurface eastward jet ($\sim$0.1 m s$^{-1}$) close to the continental slope, centered at about 200 m depth ($\sim$1.5 Sv).

### 3.1.3. Discussion of Jet Cruise circulation

The northern dipole in the dynamic height (Fig. 4d) was probably formed by the Papagayo Jet in a similar way to the Gulf of Tehuantepec dipole (Clarke, 1988; McCreary et al., 1989; Umatani and Yamagata, 1991; Barton et al., 1993; Trasviña et al., 1995; Ballestero and Coen, 2004), with the difference that in the Tehuantepec case the cyclonic eddy to the east of the wind jet most often does not develop, while in the Papagayo case it becomes the early stages of the CRD (Umatani and Yamagata, 1991; Fiedler, 2002). The anticyclonic eddy off the Gulf of Fonseca could be a young "Papagayo Eddy" (Ballestero and Coen, 2004), similar to the anticyclonic "Tehuantepec Eddies". The AVHRR-derived IR image for March 22, 1996, presented by (Ballestero and Coen, 2004, their Fig. 4) shows a young anticyclone in exactly the same place as the Fonseca eddy sampled here (Fig. 4c and d).

The temperature and salinity distributions across the Fonseca anticyclonic eddy (Fig. 6a and b; note that the top 100 m are stretched in the vertical for the salinity contours) show a deep surface mixed layer ($\sim$50 m) and upwardly concave halocline and thermocline. The diameter of this eddy is $\sim$260 km, and its depth is $\sim$150 m, both dimensions similar to those of the Tehuantepec Eddies (Barton et al., 1993; Trasviña et al., 1995). This is the first time that the internal structure of this eddy is reported.

Fig. 6c and d (section V; note that the top 100 m are stretched in the vertical for the salinity contours) show that in the center of the CRD there is practically no surface mixed layer; the thermocline is convex, with the 24–28 °C isotherms intersecting or touching the surface. The isotherms below the thermocline are shaped as a dome, with the main vertical excursion of isotherms around 150 m, and some curvature of the isolines is evident down to almost 500 m (e.g. the 8 °C isotherm). Since the geostrophic flow (Fig. 5v) is detectable to $\sim$400 m, it is possible that the CRD is deeper than 500 m. There are, on both sides of the main isotherm uplift, smaller domes indicated by isotherms 12 °C and higher, which show a small valley in the very center of the cyclonic circulation; similar features are also present in the sections presented by Wyrtki (1964) and by Barberán et al. (1985). The halocline is also convex, leading to a region of high surface salinity ($\sim$34.4) surrounded by a strong salinity front, which is strongest on the offshore side.

That the flow associated with the CRD is at least 400 m deep (Fig. 5v and vii) contradicts the idea that the CRD is a shallow ($<$100 m) feature (Kessler, 2002, 2006). This may be because Kessler (2002) is describing the climatological mean (his Fig. 7); the vertical sections from previous individual cruises (Wyrtki, 1964; the Domo cruises) show domed isotherms down to at least 500 m, in agreement with ours.

Also, we do not find the northward flow underneath the dome found by (Kessler, 2002, his Fig. 7), which he interprets as the Northern Tsuchiya Jet. This Jet (Tsuchiya, 1975; Kessler, 2006) is a

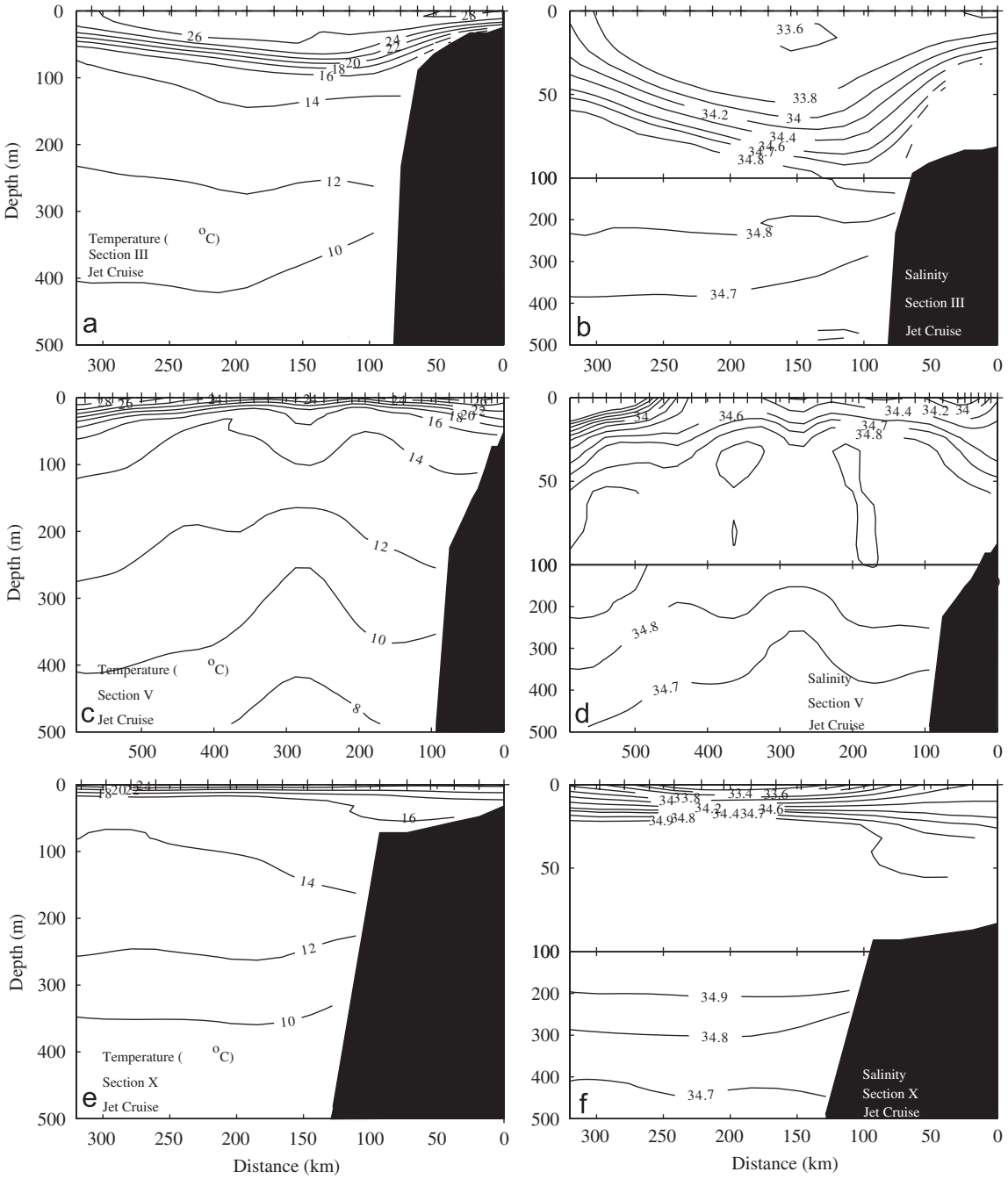


Fig. 6. Vertical sections of temperature (°C, left panels) and salinity (right panels. *Note*: the vertical axis has the top 100 m stretched in the vertical) during the Jet Cruise. (a) and (b) section III, (c) and (d) section V, (e) and (f) section X. Data were smoothed by objective analysis. Ticks in the top axis are the CTD stations.

permanent eastbound subsurface current between 4 and 5°N, at 150–400 m depth, which according to Kessler (2002, 2006) turns poleward before reaching the American Coast, flowing underneath the CRD where 3.5 of its 7 Sv transport are upwelled. The subject of the influence of the Northern Tsuchiya Jet on the CRD has previously been addressed by Voituriez (1981). He argues that since the flow around the dome is deeper than the NECC, and the NECC does not extend east of 100°W from

February to April (Tsuchiya, 1974) whereas the CRD is always present, the CRD may be created by the permanent Northern Tsuchiya Jet, rather than by the NECC. This was also the central point made by Barberán et al. (1985). The subject remains open, and our observed depth of the flow and 4–7 Sv of poleward transport associated with the CRD (Table 1, sections V and VII) are similar to those of the Northern Tsuchiya Jet. If the Northern Tsuchiya Jet influences the CRD, then the CRCC would also be influenced by it. It would be highly desirable to obtain detailed observations of the termination of the Northern Tsuchiya Jet and its relation with the CRD.

The dipole suggested by the circulation off the Gulfs of Panama and Chiriquí was only partly sampled here. However, the cyclonic circulation in the Gulf of Panama is an established feature, and for winter it is generally assumed to be generated by the Panama Jet. It was observed by Stevenson (1970) in February–March of 1966, it is present in the January to April maps of ship-drift surface circulation presented by Fiedler (2002) and it is also present in the mean January–March satellite altimeter-derived circulation of Rodríguez-Rubio et al. (2003) and in the drifter data of Chaigneau et al. (2006). The latter two references also show the dipole circulation apparent in Fig. 4d, including the southward surface flow off the Gulf of Chiriquí, which also appears in the ship-drift maps of Wyrtki (1965) and Fiedler (2002). However, the magnitude of the westward surface flow in the Gulf of Panama observed here (Fig. 5x) is weaker ($\sim$0.15 m s$^{-1}$) than the speed measured with surface drifters ($\sim$30 m s$^{-1}$) by Chaigneau et al. (2006), which is reasonable since the drifter measurements include Ekman drift.

Since there are so few observations of the hydrographic structure of the Gulf of Panama, we present the temperature and salinity of section X in Fig. 6e and f, the latter with the top 100 m stretched in the vertical. Several isotherms reach the surface establishing thermal fronts, evident in the SST (Fig. 4a), and the 16–26 °C isotherms are pressed together in the top 25 m offshore and in the top 60 m on the continental shelf. The isohalines show a similar pattern, producing a highly stratified surface layer. The evidence of upwelling includes the low SST (24 °C) and the relatively high surface salinity (34.0) at the head of the Gulf of Panama in Fig. 4b. The overall northward deepening of the 10–15 °C isotherms in Fig. 6e is responsible for the surface westward flow, and their sudden uplifts at 300 and 150 km cause the subsurface eastward flows at those positions (Fig. 5x).

Most of the sections I to VII present a coastal poleward flow (except sections III and IV because of the anticyclonic Fonseca eddy), which can be identified as the CRCC. As far as the authors know, this may be the first time that the structure of the CRCC has been reported. The picture is not simple, since there is no smooth transition from the flow around the CRD to the CRCC. The poleward flow associated with the CRD has a tortuous trajectory before reaching sections I and II. It seems more likely that the poleward flow in the offshore part of section III (Fig. 5iii), which may be due to both the Fonseca eddy and the CRD, is the origin of the poleward coastal flow in sections I and II. Although average circulation in the area from satellite altimetry (Rodríguez-Rubio et al., 2003), from the surface drifters (Chaigneau et al., 2006), and from hydrography (Kessler, 2006) is in agreement with the classical interpretation of a smooth flow, our data indicate that there is a high degree of eddy variability. Chaigneau et al. (2006) point out that the kinetic energy in the Panama Bight is dominated by eddy activity, and Trasviña and Barton (2008) find that the summer circulation in the Gulf of Tehuantepec is dominated by eddies (while the CRCC is not detectable).

The geostrophic NECC is not present in this zone at this time of the year (Tsuchiya, 1974; Kessler, 2006), but the dynamic height distribution shown in Fig. 4d suggests that there is a geostrophic eastward flow extending from the southern edge of the CRD to sections VIII and IX. There it turns south, probably because of the convergence with the westward flow from the Panama Bight. The geostrophic velocity sections (Fig. 4vi–ix) show that this eastward flow is very shallow. In agreement with the dynamic height distribution shown in Fig. 4d, the dynamic height from satellite altimeter also suggests a connection (Rodríguez-Rubio et al., 2003). In sections VIII and IX, there is westward flow underneath, whose origin is unknown, although Kessler's (2002) Figs. 8 and 10 suggest a subsurface connection with the cyclonic circulation in the Panama Bight. However, because of the wide gap between sections VII and VIII, the apparent connection could be an artefact of the interpolation scheme. More data could resolve this issue.

Novel features present in the geostrophic velocity sections are (a) the presence of a subsurface westward current over the slope and shelf in sections

VIII and IX and (b) a weak subsurface core of eastward/equatorward flow in sections I, II, and IX and in the Gulf of Panama (section X).

### 3.2. The Wet Cruise (September 25 to October 18, 1993)

#### 3.2.1. Surface distributions

The distribution of AVHRR-derived SST is shown in Fig. 3b. The ITCZ (not shown) is now in its northern position, so that in the surveyed area winds are weak and from the south or SW. The high temperatures of the Warm Water Pool are present to the northwest of the surveyed region, and are separated from cooler waters to the south by a zonal front. In the cool area, in the expected position of the CRD (Stage 3, as described before), there is a barely discernible ellipsoidal area of SST minimum.

The CTD-derived SST (Fig. 7a) shows isotherms parallel to the coast, except in the NW, where the isotherms form a thermal front oriented normal to the coast. The SST variation is small, 2 °C at most. The most salient feature is the zone with a relative minimum (~27 °C) centered on 10°N, 90°W, which we interpret as the eastern edge of the CRD, supported by the climatological CRD for this time of the year (shaded area). Also note the curvature of the 28 °C isotherm off the Gulf of Fonseca.

The surface salinity away from the coast was ~33 (Fig. 7b), with the maximum value (>33.6) coinciding with the SST minimum, supporting the identification of this area as the CRD. There is a pronounced surface salinity minimum in the Gulf of Panama ($S<28$), from which a haline front extends toward the NW, suggesting a low-salinity wedge extending poleward parallel to the coast. The low-salinity coastal waters arise from precipitation and land runoff, which peak at this time of year (Amador et al., 2006; Fiedler and Talley, 2006).

The depth of the thermocline (Fig. 7c) presents an ample minimum (~20 m) that coincides with the SST minimum and surface salinity maximum centered at 9°N, 90°W, thus further supporting the identification of this area as the CRD, which at this

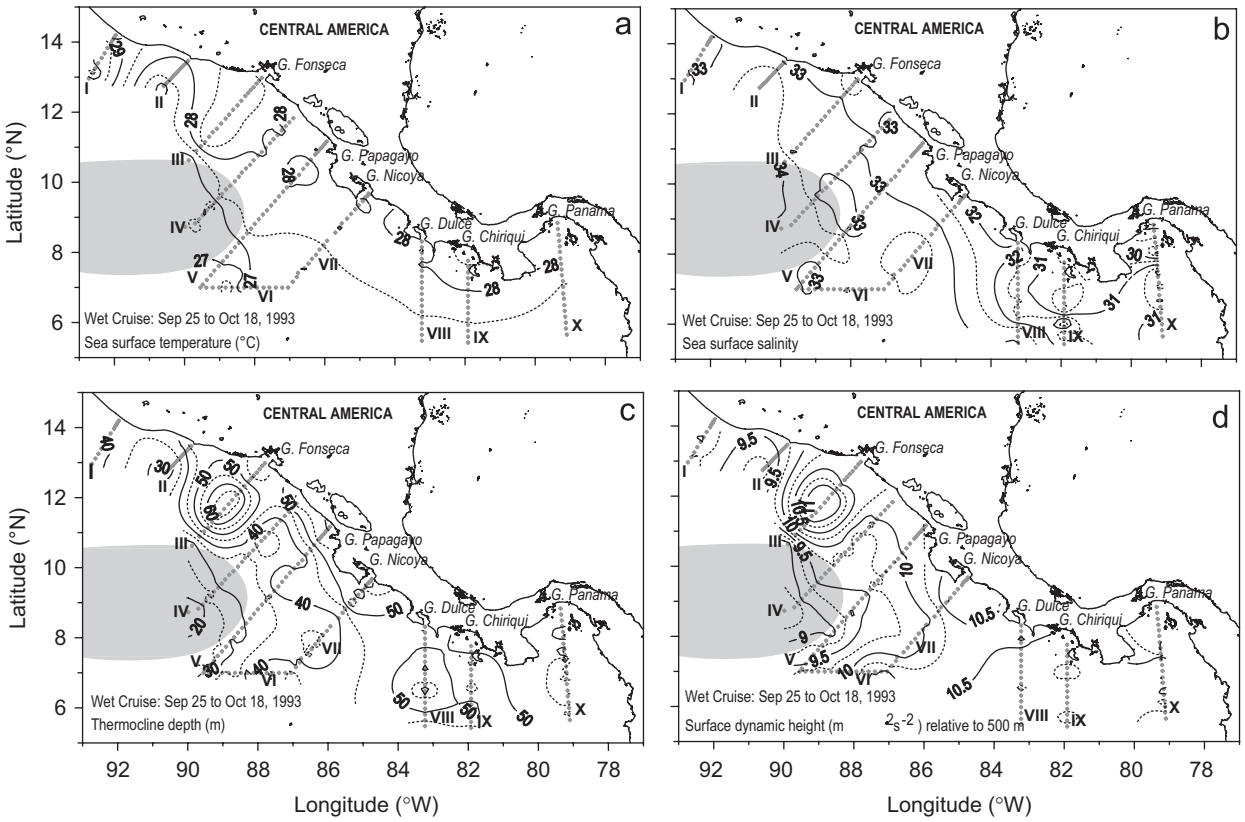


Fig. 7. Horizontal distributions during the Wet Cruise, September–October 1993. (a) SST in °C, (b) Sea surface salinity, (c) Thermocline depth in m (depth of 20 °C), (d) dynamic height of the surface relative to 500 m, in $m^2 s^{-2}$. Shading is the climatological position of the Costa Rica Dome for September, according to Fiedler (2002).

time has its maximum intensity and westward extension (Fiedler, 2002). There is also a deep circular maximum (~65 m) off the Gulf of Fonseca, revealing an eddy that was only suggested by the SST field (Fig. 7a).

The surface dynamic height (relative to 500 m) (Fig. 7d) also supports the interpretation regarding the CRD; there is an eastward flow in its southern flank, presumably the NECC since at this time of the year it is well developed (Kessler, 2006), which branches into a cyclonic flow around the CRD and a possible eastward flow. The Fonseca eddy is well defined. The poleward flow between the CRD and the coast is the start of the CRCC, but it looks less tight than in the Jest Cruise. As in the Jet Cruise, the CRCC soon encounters the anticyclonic Fonseca eddy and joins its offshore flow, thus interrupting the poleward flow.

### 3.2.2. *Vertical distribution of geostrophic velocity*

Fig. 8 shows the vertical distribution of geostrophic velocity ($V_g$) assuming no motion at the deepest common depth of adjacent stations (~900 m in the offshore stations). The sections are arranged north to south, but they will be described in the order needed for interpretation, starting with the CRD.

The flow around the CRD is described by sections V, VI and VII (Fig. 8v–vii). Section V (Fig. 8v) cuts the eastern edge of the CRD in two places (see Fig. 7d), so that the geostrophic velocity shows a well-defined cyclonic circulation, reaching down to ~500 m depth; the transport associated with the CRD is ~7 Sv (Table 1). There is surface northwestward flow in the 300 km between the CRD and the coast, transporting 6.7 Sv, although it seems separated into two cores: one over the continental shelf with maximum surface speed ~0.25 m s$^{-1}$ and depth over 100 m, and the other with maximum surface speed ~0.1 m s$^{-1}$, with depth ~100 m in most areas and ~500 m at some stations. The weakness of the flow between the CRD and the land is also evident in the isolines in Fig. 7c and d. The southeastward flow in the offshore half of section V is faster (~0.25 m s$^{-1}$), ~150 km wide, ~500 m deep, and transports 7.6 Sv. This is just the eastward component of the flow around the CRD, while its northward component, which is ~200 m deep and ~0.25 m s$^{-1}$ at the surface, is provided by the zonal section VI (Fig. 8vi). Most of section VII presents poleward surface flow (transporting 5.2 Sv), presumably after circulating around the CRD, which deepens and strengthens toward the coast, where it reaches a depth of 200 m and a speed ~0.25 m s$^{-1}$ at the surface. At the offshore end of Section VII (Fig. 8vii), there is southeastward flow with speed ~0.2 m s$^{-1}$ and 200 m deep, transporting 2.3 Sv; Fig. 7d suggests that it represents some of the flow on the south side of the CRD that turned to the east. This is quite likely since at this time the NECC is maximal, and as shown below, there is eastward flow in the offshore half of sections VIII and IX.

North of the CRD, section IV has a very complex circulation because it is in the transition area between the cyclonic flow around the CRD (Fig. 7d and Fig. 8iv) and the anticyclonic flow around the Fonseca eddy. The northeastern edge of the circulation around the CRD is shown in Fig. 8iv as a 350 m deep 0.25 m s$^{-1}$ poleward flow between 300 and 450 km; this section is almost perpendicular to the edge of the CRD. In addition, section IV shows a shallow (~100 m) northwestward coastal flow (~0.1 m s$^{-1}$) and a subsurface (50–450 m) southeastward flow (~0.1 m s$^{-1}$) between 200 and 300 km offshore. The latter may be related to the Gulf of Fonseca eddy.

The Fonseca eddy was crossed by section III (Fig. 8iii), which shows that the coastal flow due to the eddy is some 125 km wide, reaches 0.45 m s$^{-1}$ at the surface, and transports 5.7 Sv (Table 1). At 110 km offshore, this flow reaches to depths of ~300 m, but over the shelf break it is only 100 m deep, because of a subsurface poleward current (~0.05 m s$^{-1}$) attached to the continental slope and centered at ~250 m (a similar feature is found in section IV). Offshore from the center of the eddy (110 km), the northwestward flow barely exceeds 100 depth as far as 250 km, beyond which it deepens to 500 m, and the surface speed reaches 0.5 m s$^{-1}$ at the most offshore stations. This fast and deep northwestward flow is a continuation of the flow around the CRD, as indicated by the dynamic topography (Fig. 7d); it transports 9.3 Sv (Table 1).

Sections I and II (Fig. 8i and ii) show a fast (0.5 m s$^{-1}$ in the surface) coastal poleward flow. In Section II (Fig. 8ii) the poleward flow is evident above 200 m, with surface speed ~0.3 m s$^{-1}$ in the 80 km adjacent to the coast, presumably the CRCC reformed after the disruption at the Fonseca eddy; the transport of this poleward flow is ~2 Sv (Table 1). There is also a weak (0.05 m s$^{-1}$) core of poleward flow between 500 and 700 m. In section I (Fig. 8i), the poleward flow is weaker (~0.2 m s$^{-1}$) but occupies most of the section and reaches 600 m;

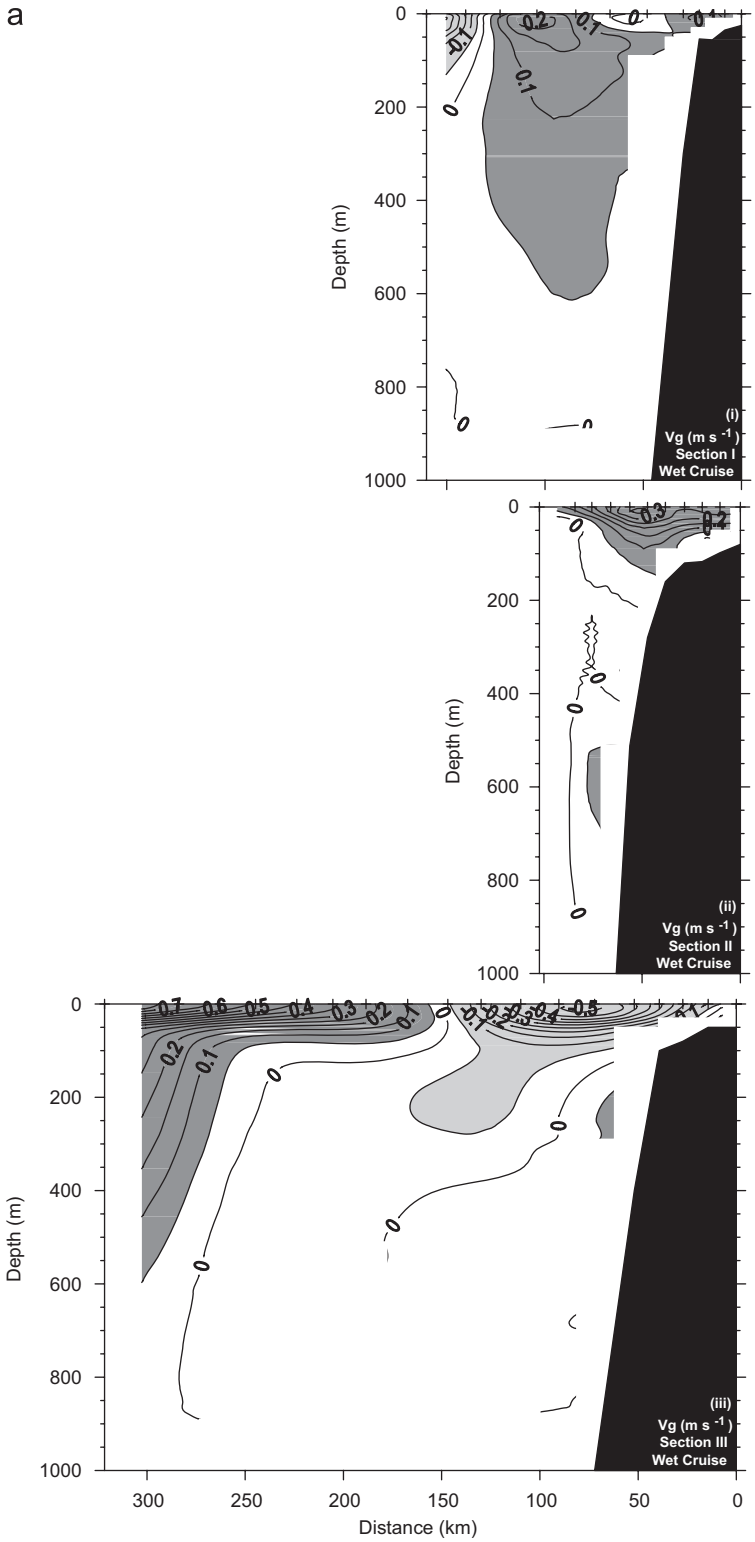


Fig. 8. Vertical distribution of geostrophic velocity ($V_g$, m s$^{-1}$) relative to deepest common depth (~900 m in deep stations), for the Wet Cruise: (i) section I, (ii) section II, (iii) section III, (iv) section IV, (v) section V, (vi) section VI, (vii) section VII, (viii) section VIII, (ix) section IX, (x) section X. Positive velocity (into the page) above 0.05 m s$^{-1}$ is shaded. Ticks in the top axis are the CTD stations.

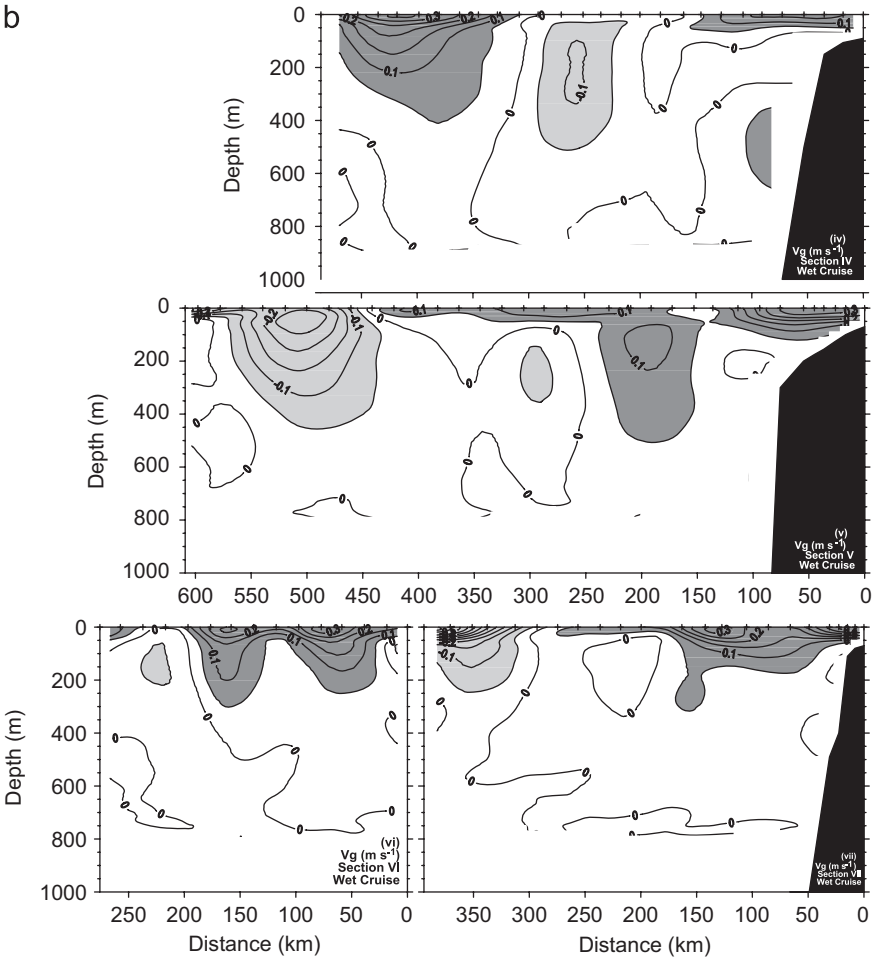


Fig. 8. (*Continued*)

the poleward transport is 3.6 Sv (Table 1). Offshore from 120 km, some equatorward flow is present in the upper 100 m.

The dynamic height (Fig. 7d) suggests that a branch of the eastward flow on the southern side of the CRD continued flowing eastward as part of the NECC. In section VIII (Fig. 8viii) there is eastward flow in the southern part of the section reaching to 500 m in some places, with mean speed $\sim 0.1\,m\,s^{-1}$ and transport ~7.9 Sv. Westward flow is found between 50 and 150 km from the coast, with mean speed $\sim 0.1\,m\,s^{-1}$ down to 700 m depth; it transports 10.9 Sv (Table 1). In the 50 km close to the coast, weak ($0.05\,m\,s^{-1}$) eastward flow is found. In Section IX (Fig. 8ix) there is also eastward flow in the offshore ~150 km, with speed $\sim 0.2\,m\,s^{-1}$and ~200 m deep. In the northern part of the section, the flow is westward, with speed up to $0.25\,m\,s^{-1}$ on the shelf and $\sim 0.1\,m\,s^{-1}$ on the slope; the depth of this westward current is ~450 m, and its transport is 3.6 Sv (Table 1).

In the Gulf of Panama (section X, Fig. 9x) there is mostly westward flow, adjacent to the continental shelf and slope and reaching ~600 m. The speed is $\sim 0.3\,m\,s^{-1}$ at the surface on the shelf, and there is a second maximum $> 0.3\,m\,s^{-1}$ at ~200 m depth; the westward transport is quite high, at 8.5 Sv (Table 1). This flow structure does not agree with the description of Stevenson (1970), who indicated that the cyclonic flow in the Panama Bight did not extend deeper than 100 m.

### 3.2.3. Discussion of Wet Cruise circulation

The circulation between the CRD and the coast was weaker and shallower than in the Jet Cruise. In both north and south it was deeper and faster than in the east; in the south because of the NECC and in the north because of the Fonseca Eddy, which again

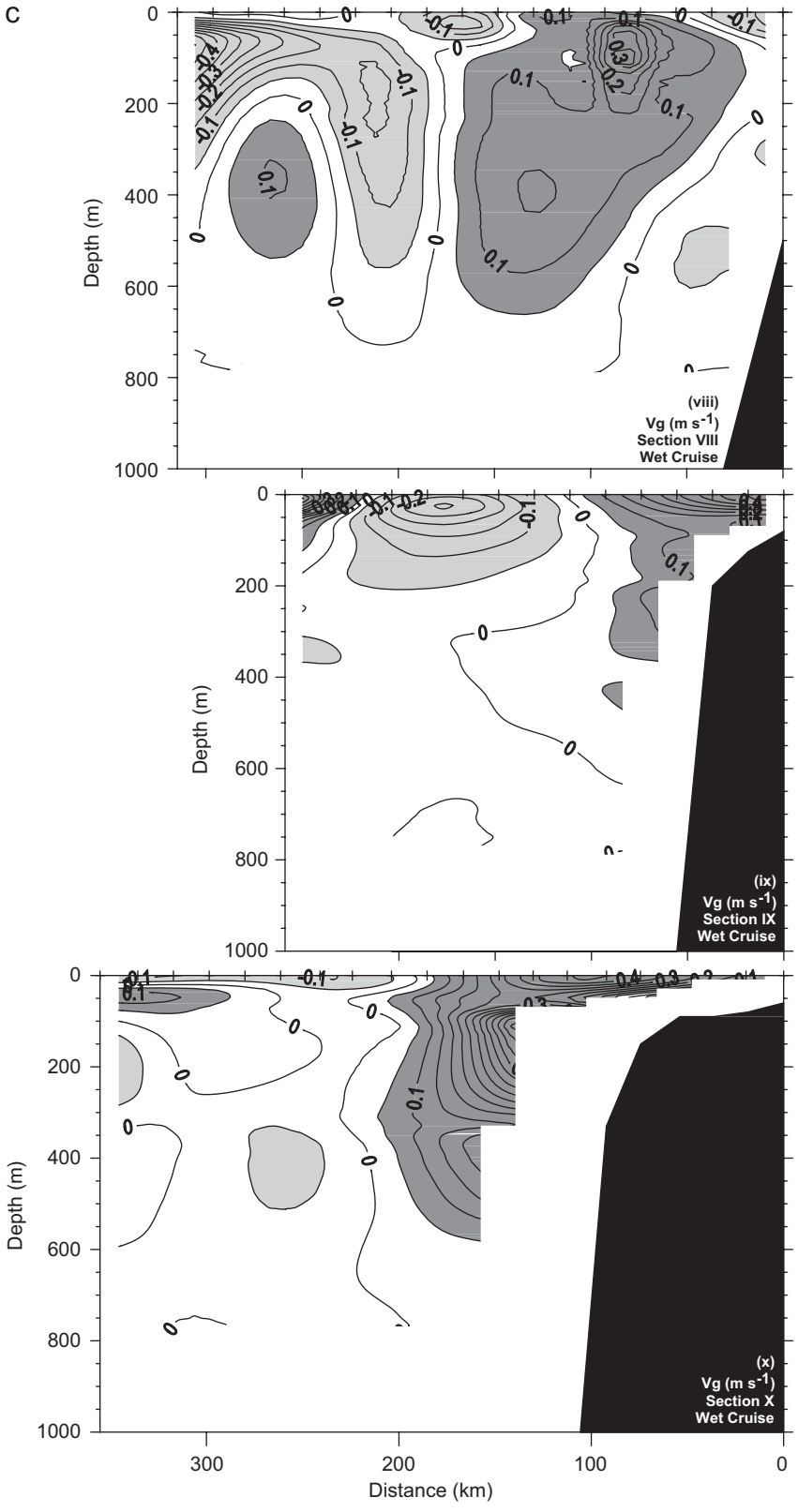


Fig. 8. (*Continued*)

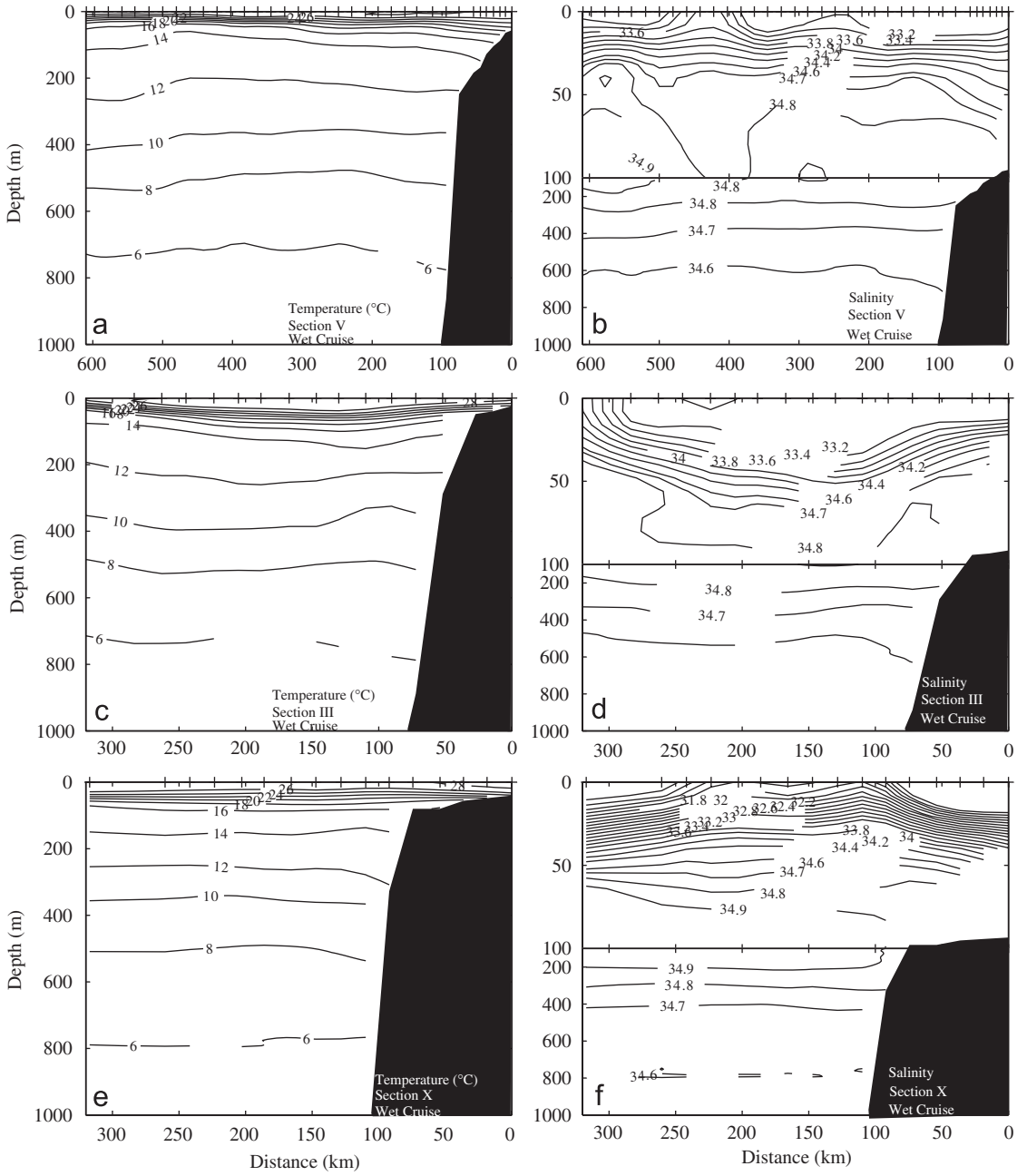


Fig. 9. Vertical sections of temperature (°C, left panels) and salinity (right panels. Note: the top 100 m are stretched in the vertical) during the Wet Cruise, for (a) and (b) section V, (c) and (d) section III, (e) and (f) section X. Data were smoothed by objective analysis. Ticks in the top axis are the CTD stations.

interrupted the northwestward flow of the coastal current. However, volume transports during the Wet Cruise are higher than during the Jet Cruise (Table 1); this could be because of the depth to which sampling was done: 500 m in the Jet Cruise and 900 m in the Wet Cruise. To show the importance of the maximum sampling depth, the transport during the Wet Cruise was also calculated for the top 500 m, taking the level of no motion at 500 m (second row in Table 1): not counting sections I and VI, the transport is lower by a factor of 0.5–0.86. It is therefore important that in future surveys sampling should be done to at least 1000 m depth.

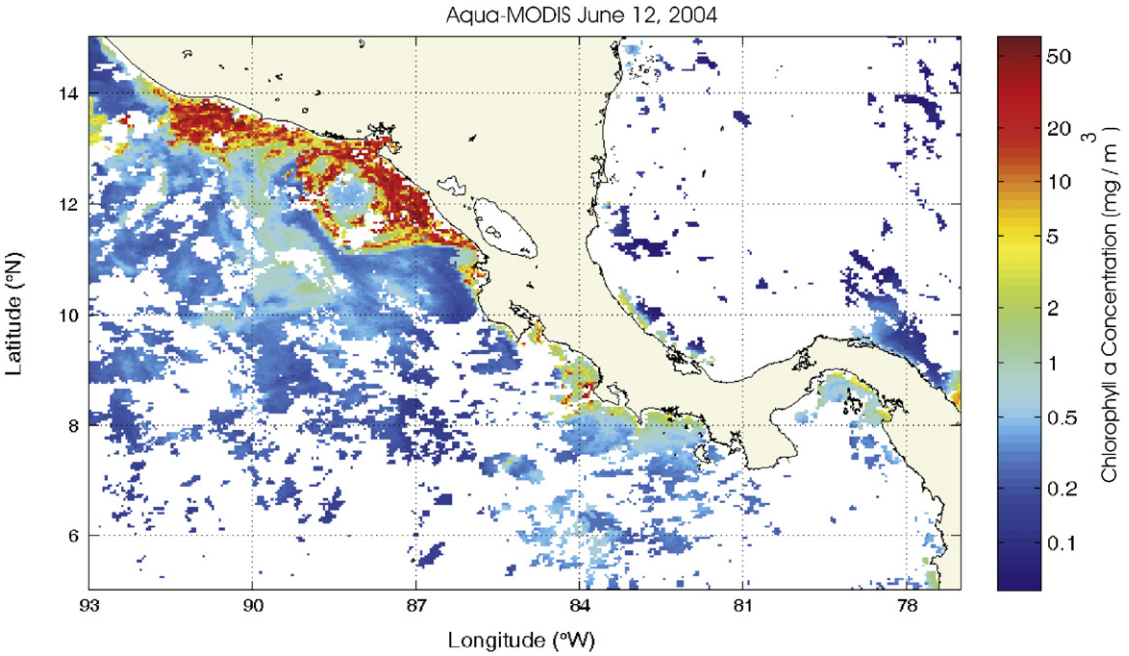


Fig. 10. Chlorophyll (mg m$^{-3}$) satellite image (Aqua-MODIS) for June 12, 2004, showing a summer anticyclone off the Gulf of Fonseca. Data downloaded from http://oceancolor.gsfc.nasa.gov/cgi/level3.pl.

The thermohaline structure of the CRD is shown by section V (Fig. 9a and b). The thermocline isotherms (Fig. 9a) are crowded together close to the offshore end of the section, from where they spread out and tilt down toward the coast; the halocline shows the same pattern (Fig. 9b). The isotherms $<13\,^{\circ}C$ present a dome shape, but not very pronounced because the section crossed the dome almost at its edge, as shown by Fig. 7c and d. The isohalines (Fig. 9b) are very crowded in the surface layer, in order to accommodate the low-salinity values there. The slope of the isotherms (Fig. 9a) is weak between the CRD and the shelf, leading to the weak shallow flow seen in Fig. 8v. Over the shelf, however, the flow was associated with a sudden deepening of the thermocline toward the land mass. The sharpest tilt of the isotherms is in the southwest of section V, where some of the structure is most likely associated with the NECC, which at this time of year flows eastward toward the Panama Bight (Rodríguez-Rubio et al., 2003; Kessler, 2006; Chaigneau et al., 2006).

The warm Fonseca eddy was located in exactly the same position as in the Jet Cruise (compare Fig. 4c, d and Fig. 7c, d); it was very well defined and associated with thermocline and halocline depressions. It is unlikely that it is the same eddy seen in the Jet Cruise, since such eddies typically drift westward (Willett et al., 2006). The temperature and salinity distributions for Section III (Fig. 9c and d), which crossed the Fonseca anticyclonic eddy, look remarkably like those in the Jet Cruise (Fig. 6a and b), with a lenticular surface mixed layer and concave thermocline and halocline underneath. Differences are that now the thermocline and halocline are shallower and weaker, and the surface layer is thinner (~30 m), warmer ($>28\,^{\circ}C$) and fresher (32.9–33.0) than in the Jet Cruise. The deep isotherms are concave down to ~500 m. Like in the Jet Cruise, the diameter of the Fonseca eddy was around 250 km, and its depth was less than 150 m. The equatorward transport of the eddy was ~5.5 Sv on both occasions (Table 1, Section III).

While the genesis of the Fonseca Eddy in winter could be associated with the Papagayo Jet (e.g., Ballestero and Coen, 2004), the forcing for the summer is not obvious. The presence of anticyclonic eddies off Central America during summer, or in the absence of wind forcing, has been reported both in observations and in numerical models. Fig. 10 shows a rare image (the area is usually cloud-covered through the summer) showing one such eddy in the chlorophyll image of the AQUA MODIS sensor for June 12, 2004; it is located in exactly the same place as the Fonseca eddy

described here. Brenes et al. (1998) found evidence of a warm eddy during summer in a seasonal composite of hydrographic data collected monthly off the coast of Nicaragua between 1984 and 1988. Hansen and Maul (1991) observed a satellite-tracked drifter trapped in an anticyclone that most likely was formed off Central America in the summer of 1987. These authors suggested that such summer anticyclonic eddies could be formed due to total vorticity conservation: as the NECC turns north along the coast, anticyclonic relative vorticity must be gained to balance the change in planetary vorticity. An alternative generation mechanism for the Fonseca eddy is current instability: the numerical model of Umatani and Yamagata (1991) produced an anticyclone without wind forcing, which they explained as instability of the surface currents. Trasviña and Barton (2008) suggest that even summertime weak cross-isthmus winds may be important. Zamudio et al. (2001, 2006) used satellite altimeter data and numerical model results to argue that coastal-trapped waves can induce instability in the coastal current off SE Mexico and trigger the formation of gyres, especially during El Niño conditions. The data presented here suggest that this eddy is closely related to the flow around the CRD, as their currents seem to be intimately interwoven (Fig. 7d and Fig. 8iii, iv).

The coastal poleward flow is more complicated than the climatological analyses suggest, making it hard to define the CRCC. In addition to the northwestward flow over the shelf, which may be buoyancy-driven by fresh water input from river runoff, as suggested by the distribution of surface salinity (Fig. 7b), in most of Fig. 8 there is a deeper (surface to 300–600 m) poleward flow attached to the continent. For sections east and north of the CRD this flow would be identified as the CRCC, and for section X it could be explained as part of the cyclonic circulation of the Panama Bight. However, its presence in sections VIII and IX, transporting 10.9 and 3.6 Sv, respectively, is unexpected. It cannot be generated by the NECC nor by the Colombia Current, because they are both shallower than 100 m (Stevenson, 1970). However, the dynamic height at 300 m relative to 450 m for this zone (Fig. 10 of Kessler, 2002) suggests a subsurface flow extending west from the Panama Bight following the shape of the coast. As mentioned before, another possible source of deep poleward flow is the Northern Tsuchiya Jet (Tsuchiya, 1975), and since observations suggest that the Southern Tsuchiya Jet turns south at the eastern boundary to feed the Peru-Chile undercurrent and countercurrent (Lukas, 1986), it is possible that something similar happens in the north. This feature clearly requires further research.

As mentioned above, the westward flow in the Gulf of Panama (Fig. 8x) is much deeper than the 100 m claimed by Stevenson (1970) for the Colombia Current, and it transports 8.5 Sv (Table 1); however, it agrees with Kessler's (2002) Fig. 10, which shows considerable rise of the dynamic height (at 300 m relative to 450 m) toward the coast around the bight's periphery. The thermohaline structure for section X (Fig. 9e and f) shows that the deep westward flow is due to a sudden upward and then downward sloping of the isolines in the 50 km closest to the continental slope. Our observations of westward flow in the northern part of the Gulf of Panama and west of it are in disagreement with the July–September circulation obtained by Rodríguez-Rubio et al. (2003) from satellite altimetry, but in agreement with the satellite-tracked drifter study of Chaigneau et al. (2006).

## 4. Conclusions

Hydrographic CTD observations are used to describe the geostrophic circulation between the CRD and Central America for the seasons of (a) February–March (1994) when the transcontinental wind jets are near their peak, and (b) September–October (1993) when precipitation is maximum, but the winds are weak.

In February–March 1994 the CRD was a closed ring ~500 km in diameter attached to the coast. It was at least 400 m deep, had a geostrophic surface speed ~0.25 m s$^{-1}$ and transported ~7 Sv. The Dome had a cyclonic circulation in the 150 km around the rotation axis, with subsurface maximum speed (0.15–0.20 m s$^{-1}$) at ~180 m depth; the associated uplift of the isotherms was ~150 m. The isotherms presented convexity at the maximum sampled depth of 500 m, suggesting that the flow extended deeper. On the southern edge of the CRD the speed at the surface reached 0.45 m s$^{-1}$, and part of that flow appears to have continued eastward toward the Panama Bight as a shallow surface current, although the geostrophic NECC is not present at this time of the year. Over the shelf the poleward flow was ~100 m deep with speed ~0.2 m s$^{-1}$.

In September–October 1993, the eastern edge of the CRD was found ~450 km from the coast. The

current between the dome and the coast was mostly ~100 m deep and weak (~0.15 m s$^{-1}$), but on the southern side it was deeper (~450 m) and faster at 0.3 m s$^{-1}$, presumably because of the presence of the NECC. Over the shelf, the flow was ~150 m deep, it had a surface speed ~0.25 m s$^{-1}$ and the transport was ~7 Sv.

Off the Gulf of Fonseca, a warm anticyclonic eddy was found, both in winter and summer; its position, diameter (~250 km), depth (~150 m), surface speed (~0.5 m s$^{-1}$), and transport (~5.5 Sv) were almost identical on the two occasions. The circulation of this eddy was interwoven with that of the CRD. It appears in AVHRR images more clearly in winter, but sometimes it is also seen in summer chlorophyll images. Although in winter it may be due to the convergence on the poleward side of the Papagayo Jet, the fact that its characteristics are so similar in both seasons suggests that a less seasonal mechanism may be at play, like instability of the coastal flow related to the passage of coastally trapped waves (Zamudio et al., 2006), or vorticity conservation (Hansen and Maul, 1991).

The dynamic height in September–October shows part of the NECC flowing eastward south of the CRD and branching into a poleward deflection between the dome and the Central American coast, and an eastward flow toward the Panama Bight.

Poleward flow was observed over the shelf and slope in both seasons, and throughout the sampled domain, which covers all Central America. In both occasions it was interrupted and forced offshore by the anticyclone in the Gulf of Fonseca. This poleward coastal flow was expected for the area north of the CRD, where it can be identified as the CRCC. However, the transition from flow around the CRD to the CRCC was quite tortuous because of the presence of mesoscale eddies (like the Fonseca eddy). There may be an influence of the low salinity from runoff on the flow near the coast during the rainy season.

In the Panama Bight (section X) westward flow was also expected, but not as deep as 600 m and transporting 8.5 Sv, as observed in September–October, nor its apparent continuation to the two sections immediately to the west (VIII and IX). In the February–March cruise, the westward flow was weaker and shallower than in September–October. In the February–March cruise, below the westward cores in sections VIII, IX and X there were subsurface cores of eastward flow attached to the continental slope.

To the authors' knowledge, there are no other direct observations as detailed as these of the circulation and hydrographic structure of this zone. Therefore, in addition to adding details to overall patterns known from Wyrtki's observations and from constructed climatologies, some novel features were encountered; these findings need support from independent sources, and a more satisfactory integration with the body of knowledge of the regional oceanography.

## Acknowledgments

This work was possible thanks to the support of several agencies. PRADEPESCA funded the work at sea. In Costa Rica, the work was funded by Universidad Nacional de Costa Rica, via Servicio Regional de Información Oceanográfica, and in Mexico by UABC via funding for IIO, and by the Federal Government through CICESE. The participation of M.F.L. is part of CONACyT contracts D41881-F and SEP-2003-C02-42941/A-1, and some of his work was done while he was recipient of a UC-MEXUS sabbatical at SIO-UCSD, hosted by Prof. P. Niiler. This paper is a contribution to the scientific agenda of EPCOR (IAI). Dr. P. Fiedler kindly provided the climatological position of the CRD. We thank Drs. Rubén Castro and Emilio Beier for discussions and help with objective analysis techniques. Drs. A. Badan and E.D. Barton made extensive comments and corrections that significantly improved this article. Technical support was provided by V. Godínez, C. Cabrera, and S. Larios.

## References

Amador, J.A., Alfaro, E.J., Lizano, O.G., Magaña, V.O., 2006. Atmospheric forcing of the eastern tropical Pacific: a review. Progress in Oceanography 69, 101–142.

Ballestero, D., Coen, J.E., 2004. Generation and propagation of anticyclonic rings in the Gulf of Papagayo. International Journal of remote Sensing 25 (11), 2217–2224.

Barberán, J.M., Gallegos, A., Fernández, A., Mee, L.D., 1985. Subsurface origin of the Costa Rica Dome. Unpublished manuscript.

Barton, D., Argote, M.L., Brown, J., Kosro, M., Lavín, M.F., Robles, J.M., Smith, R.L., Trasviña, A., Vélez, H.S., 1993. Supersquirt: dynamics of the Gulf of Tehuantepec, México. Oceanography 6, 23–30.

Brenes, C., Hernández, A., Gutiérrez, A., 1998. Sea surface thermohaline variations along the Nicaraguan Pacific coastal waters, vol. 5(1). Tópicos Metorológicos y Oceanográficos, Instituto Meteorológico Nacional, San José, Costa Rica, pp. 17–26.

Chaigneau, A., Abarca del Rio, R., Colas, F., 2006. Lagrangian study of the Panama Bight and surrounding regions. Journal of Geophysical Research 111, C09013.

Chelton, D.B., Esbensen, S.K., 2000. Satellite observations of the wind jets off the Pacific coast of Central America. Part II: regional relationships and dynamical considerations. Monthly Weather Review 128, 2019–2043.

Chelton, D.B., DeSzoeke, R.A., Schlax, M.G., Naggar, K.E., Siwertz, N., 1998. Geographical variability of the first baroclinic Rossby radius of deformation. Journal of Physical Oceanography 28, 433–460.

Chelton, D.B., Freilich, M.H., Esbensen, S.K., 2000. Satellite observations of the wind jets off the Pacific coast of Central America. Part I: case studies and statistical characteristics. Monthly Weather Review 128, 1993–2018.

Chelton, D.B., Schlax, M.G., Freilich, M.H., Milling, R.F., 2004. Satellite measurements reveal persistent small-scale features in ocean winds. Science 303(5660), 978–983. Epub 2004 Jan 15.

Clarke, A.J., 1988. Inertial wind path and sea surface temperature patterns near the gulf of Tehuantepec and the Gulf of Papagayo. Journal of Geophysical Research 93, 15,491–15,501.

Fiedler, P., 2002. The annual cycle and biological effects of the Costa Rica Dome. Deep-Sea Research I 49, 231–338.

Fiedler, P., Talley, L., 2006. Hydrography of the eastern Pacific: a review. Progress in Oceanography 69, 143–180.

Hansen, D.V., Maul, G.A., 1991. Anticyclonic current rings in the eastern tropical Pacific Ocean. Journal of Geophysical Research 96, 6965–6979.

Kessler, W.S., 2002. Mean three-dimensional circulation in the northeast tropical Pacific. Journal of Physical Oceanography 32, 2457–2471.

Kessler, W.S., 2006. The circulation of the Eastern Tropical Pacific: a review. Progress in Oceanography 69, 181–217.

Lukas, R., 1986. The termination of the equatorial undercurrent in the eastern Pacific. Progress in Oceanography 16, 63–90.

McCreary, J.P., Lee, H.S., Enfield, D.B., 1989. Response of the coastal ocean to strong offshore winds: with applications to circulations in the gulf of Tehuantepec and Papagayo. Journal of Marine Research 47, 81–109.

Rodríguez-Rubio, E., Schneider, W., Abarca del Río, R., 2003. On the seasonal circulation within the Panama Bight derived from satellite observations of wind, altimetry and sea surface temperature. Geophysical Research Letters 30, 1410.

Stevenson, M., 1970. Circulation in the Panama Bight. Journal of Geophysical Research 75, 659–672.

Trasviña, A., Barton, E.D., 2008. Summer circulation in the Mexican Tropical Pacific. Deep-Sea Research I, in press, doi:10.1016/j.dsr.2008.02.002.

Trasviña, A., Barton, E.D., Brown, J., Velez, H.S., Kosro, P.M., Smith, R.L., 1995. Offshore wind forcing in the gulf of Tehuantepec, Mexico: the asymmetric circulation. Journal of Geophysical Research 100 (C10), 20,649–20,663.

Tsuchiya, M., 1974. Variation of the surface geostrophic flow in the eastern intertropical Pacific Ocean. Fisheries Bulletin 72 (4), 1075–1086.

Tsuchiya, M., 1975. Subsurface countercurrents in the eastern equatorial Pacific. Journal of Marine Research 33 (Suppl.), 145–175.

Umatani, S., Yamagata, T., 1991. Response of the eastern Tropical Pacific to meridional migration of the ITCZ: the generation of the Costa Rica Dome. Journal of Physical Oceanography 21, 346–363.

Voituriez, B., 1981. Northern and southern equatorial undercurrents and the formation of tropical thermal domes. Oceanologica Acta 4, 497–506.

Wang, C., Enfield, D.B., 2001. The tropical Western Hemisphere warm pool. Geophysical Research Letters 28, 1635–1638.

Wang, C., Enfield, D.B., 2003. A further study of the tropical Western Hemisphere warm pool. Journal of Climate 16, 1476–1493.

Willett, C.S., Leben, R.R., Lavín, M.F., 2006. Eddies and tropical instability waves in the eastern tropical pacific: a review. Progress in Oceanography 69, 218–238.

Wyrtki, K., 1964. Upwelling in the Costa Rica Dome. Fishery Bulletin 63 (2), 355–372.

Wyrtki, K., 1965. Surface currents of the eastern tropical Pacific Ocean. Inter-American Tropical Tuna Comission Bulletin 9 (5), 271–304.

Wyrtki, K., 1966. Oceanography of the Eastern equatorial Pacific Ocean. Oceanography and Marine Biology Annual Review 4, 33–68.

Wyrtki, K., 1967. Circulation and water masses in the eastern equatorial Pacific Ocean. International Journal of Oceanology and Limnology 1 (2), 117–147.

Zamudio, L., Leonardi, A.P., Meyers, S.D., O'Brien, J.J., 2001. ENSO and eddies on the southwest coast of Mexico. Geophysical Research Letters 28, 13–16.

Zamudio, L., Hulburt, H.E., Metzger, E.J., Morley, S.L., O'Brien, J.J., Tilburg, C., Zavala-Hidalgo, J., 2006. Interannual variability of Tehuantepec eddies. Journal of Geophysical Research 111, C05001.